01 Jan 2023

Additive Manufacturing Of (MgCoNiCuZn)O High-entropy Oxide Using A 3D Extrusion Technique And Oxide Precursors

Ruoyu Chen

Saisai Li

Qingfeng Yan

Haiming Wen
Missouri University of Science and Technology, wenha@mst.edu

Recommended Citation

R. Chen et al., "Additive Manufacturing Of (MgCoNiCuZn)O High-entropy Oxide Using A 3D Extrusion Technique And Oxide Precursors," *Ceramics International*, Elsevier, Jan 2023.
The definitive version is available at https://doi.org/10.1016/j.ceramint.2023.08.061

Ceramics International xxx (xxxx) xxx

Contents lists available at ScienceDirect

Ceramics International

journal homepage: www.elsevier.com/locate/ceramint

Short communication

Additive manufacturing of (MgCoNiCuZn)O high-entropy oxide using a 3D extrusion technique and oxide precursors

Ruoyu Chen [a,b], Saisai Li [c,*], Qingfeng Yan [c], Haiming Wen [b,**]

[a] School of Metallurgical Engineering, Anhui University of Technology, Maanshan, Anhui, 243002, China
[b] Department of Materials Science and Engineering, Missouri University of Science and Technology, Rolla, MO, 65409, USA
[c] School of Materials Science and Engineering, Anhui University of Technology, Maanshan, Anhui, 243002, China

ARTICLE INFO

Handling Editor: Dr P. Vincenzini

Keywords:
High-entropy oxide
Extrusion
Additive manufacturing
Rheology
Complex geometries

ABSTRACT

This report presents an additive manufacturing approach, for the first time, to producing high-entropy oxides (HEOs) using a 3D extrusion-based technique with oxide precursors. The precursors were prepared by a wet chemical method from sulfates. Additives were utilized to optimize the rheological properties of the printing inks with these precursors, and the properties of the printed HEOs were improved by increasing the solid content of the inks. When ink with a solid content of 78 wt% was used for printing, the resulting HEO exhibited a relative density of 92% and a high dielectric constant after undergoing pressureless sintering at 800 °C. Compared to traditional methods of manufacturing HEOs, the 3D extrusion technique is a very promising method for producing HEOs with complex geometries.

Li doped (MgCoNiCuZn)O is a high-entropy oxide (HEO) that possesses significant properties, making it suitable for various applications in the energy production and storage fields [1]. A few techniques for manufacturing HEOs, such as dealloying method [2], spark plasma sintering [3], molten salt method [4], wet chemical method [5], and water oxidation [6], have been developed to date. Nonetheless, these methods encounter challenges in producing specific required geometries, restricting the applications of HEOs. In contrast, additive manufacturing techniques are attractive for applications demanding complex geometries. Recently, the use of additive manufacturing in producing ceramic materials like metal oxides and carbides has gained popularity [7]. The 3D extrusion-based additive manufacturing technique is a relatively straightforward approach that enables to design and produce parts with complex structures rapidly by depositing layers of extruded ink [8]. With inks of excellent rheology, alumina ceramic parts have been produced using the 3D extrusion process. Additionally, by optimizing the rheological behavior of inks, SiC ceramic parts with complex geometries were produced with high accuracy via the 3D extrusion process [9]. However, no studies exist on the manufacturing of HEOs via 3D extrusion-based methods. Moreover, it has been a challenge to achieve satisfactory structural strength and high density of the printed HEOs.

To address the knowledge gaps identified above, this work utilized oxide precursors prepared through a modified chemical method to develop printing ink. $(MgCoNiCuZn)_{0.7}Li_{0.3}O$ HEO specimens were then manufactured using a 3D extrusion-based approach coupled with pressureless sintering. The rheological behavior of inks affected the printability of inks and the accuracy of the final product's structure. Therefore, our study evaluated and optimized the rheology of inks. Oxide precursors were prepared through a wet chemical method using sulfates ($NiSO_4{\cdot}5H_2O$, $CoSO_4{\cdot}6H_2O$, $MgSO_4{\cdot}7H_2O$, $ZnSO_4{\cdot}7H_2O$, and $CuSO_4{\cdot}5H_2O$) and sodium hydroxide. The sulfates with a calculated equimolar ratio of metal elements were mixed in distilled water. Then NaOH solution (10 wt%) was added into mixtures solution to introduce the formation of coprecipitates. The co-precipitates were then repeatedly centrifuged and washed to remove SO_4^{2-} ions from the precipitate. Then co-precipitated were dried at 100 °C for 24h, then follow treated at 450 °C for 1h to form oxide precursors. These precursors and Li_2CO_3 were then used to prepare inks, along with a dispersant (FS20) and a binder (sodium alginate). The inks, with a solid content between 77 and 79 wt%, were planetary ball milled for 1 h. The printed green bodies were heated at 3 °C/min to 800 °C for 3 h using a conventional pressureless sintering in a box furnace and then cooled naturally to room temperature.

* Corresponding author.
** Corresponding author.
E-mail addresses: lisaisai@ahut.edu.cn (S. Li), wenha@mst.edu (H. Wen).

https://doi.org/10.1016/j.ceramint.2023.08.061
Received 18 July 2023; Received in revised form 29 July 2023; Accepted 4 August 2023
Available online 6 August 2023

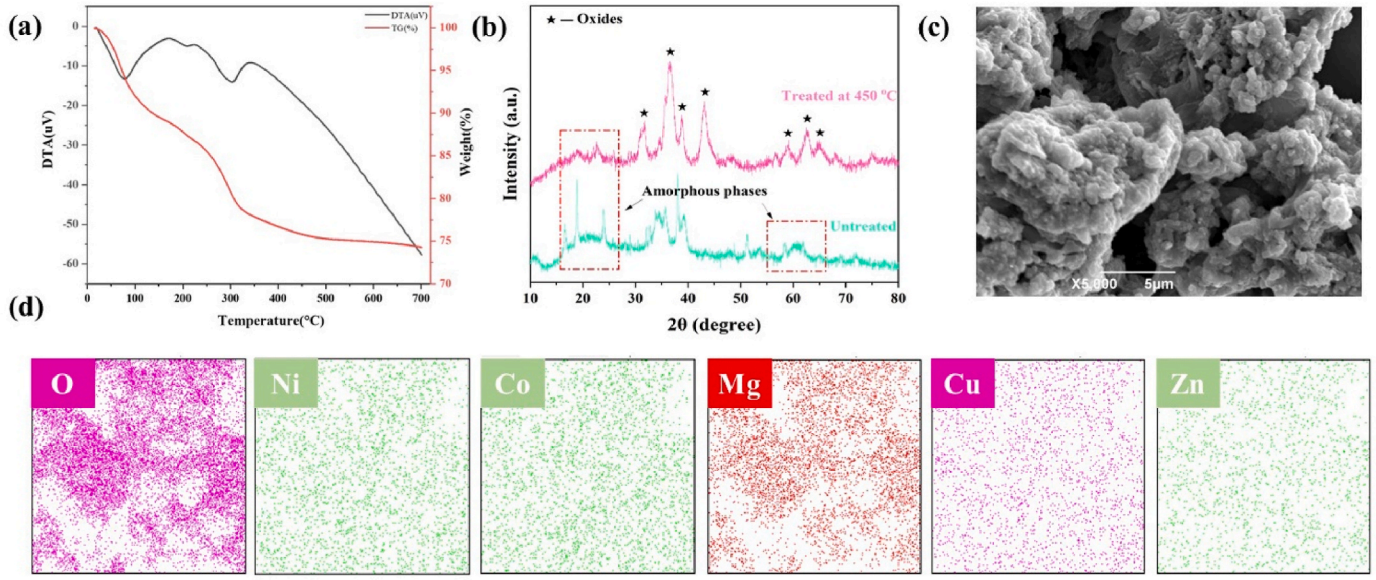

Fig. 1. The phase compositions and morphology of oxide precursors treated at 450 °C (a) thermal analysis (TGA-DTA); (b) XRD patterns; (c) SEM image; (d) EDS mapping.

Thermal analysis of the oxide precursor was performed using combined thermogravimetric differential thermal analysis (TG/DTA). A rheometer (Anton Paar MCR 102) was used to characterize the viscosity and viscoelastic properties of the inks. Thixotropic index is a ratio of an ink's viscosity at two different shear rates, generally different by a factor of ten. This value is indicative of an ink's ability to rebuild its structure. In this work, the thixotropy of inks was evaluated by using the thixotropic index γ (Equation (1)) [9]:

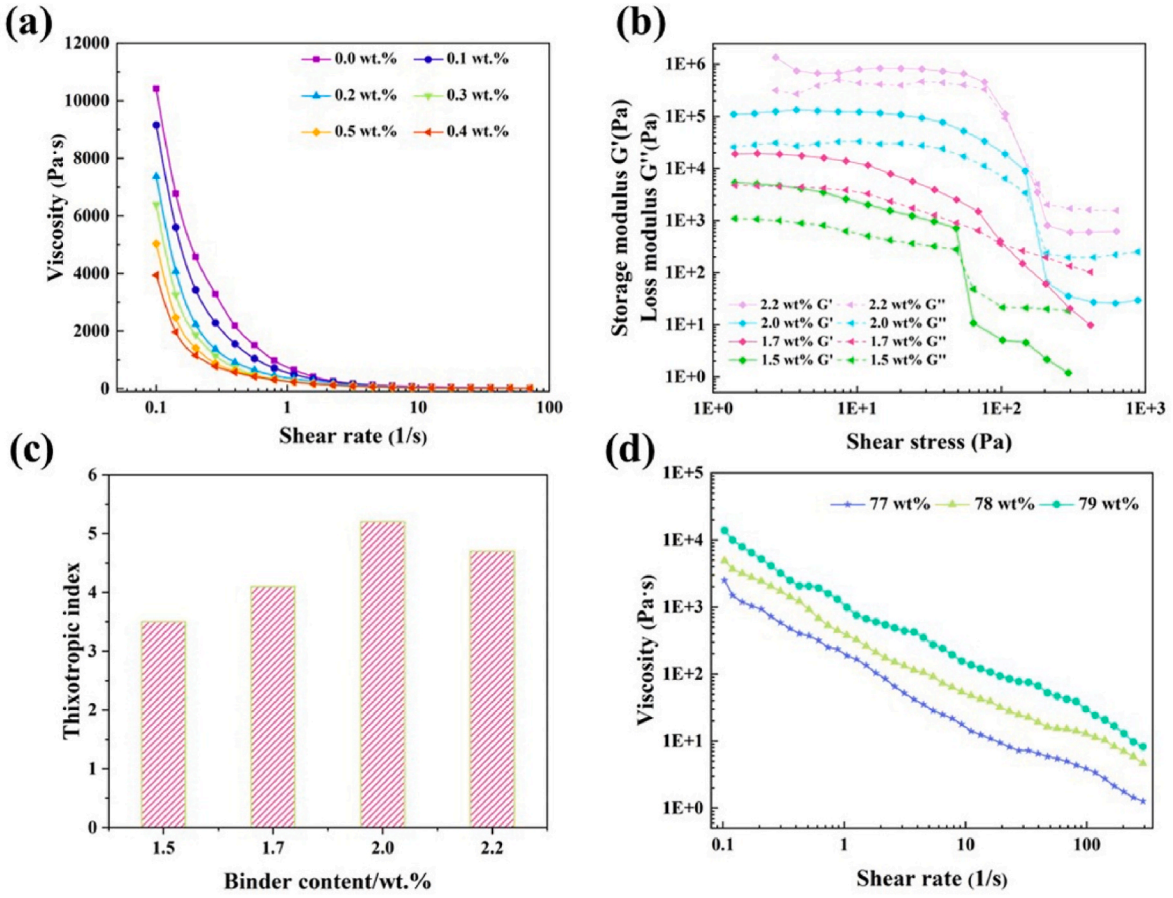

Fig. 2. Rheological behavior of the printing inks: (a) viscosity of inks with different dispersant contents; (b) viscoelasticity of inks with different binder contents; (c) thixotropic index of inks with different binder contents; (d) viscosity of inks with different solid contents.

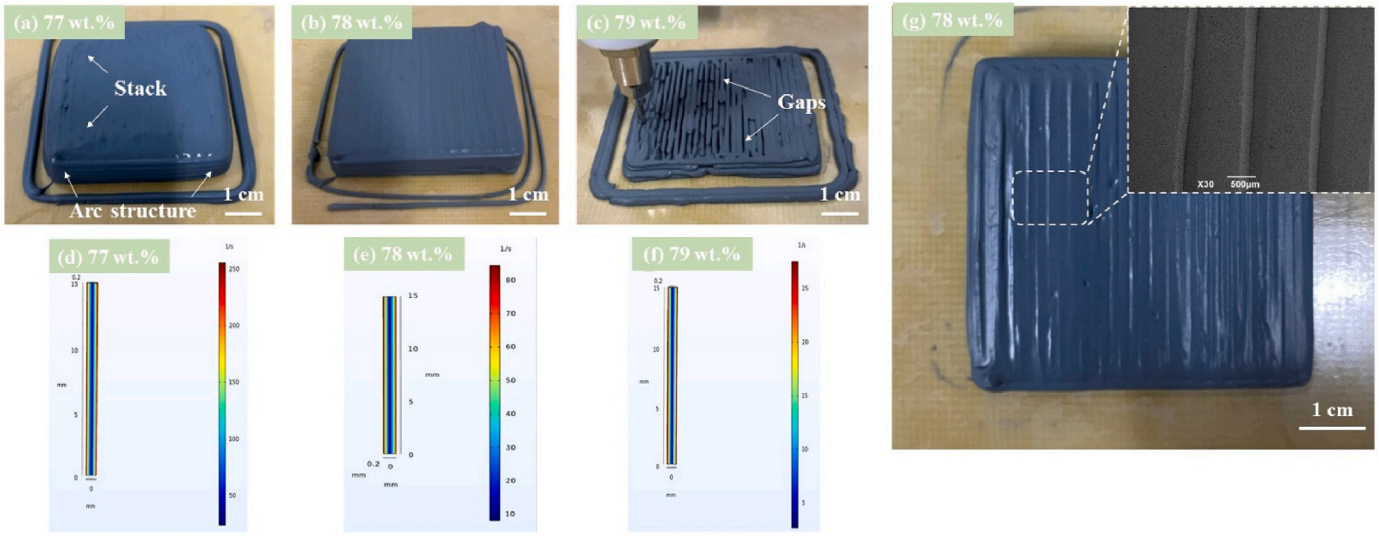

Fig. 3. (a–c) Photos showing effect of solid content on the flow behavior of ink; (d–f) COMSOL model of ink flow rate with different solid contents; (g) green body printed with a solid content ~78 wt%. (For interpretation of the references to colour in this figure legend, the reader is referred to the Web version of this article.)

$$\gamma = \frac{\tau_1}{\tau_2} \quad (1)$$

where τ_1 is viscosity at a low shear rate; in this work 5.012 s^{-1} was used. τ_2 represents an increased shear rate, with 50.12 s^{-1} being used for this work. The Archimedes method was employed to determine the density and porosity of the HEO samples, and an agilent impedance analyzer (HP4294A) was used to measure their dielectric properties at room temperature. X-ray diffraction (XRD, Philips X'Pert MRD) was utilized to determine the phase composition of the precursors and HEO samples. Finally, the microstructures of the oxide precursors and HEO were analyzed using scanning electron microscopy (JSM-6490LV) and (NANO SEM430), respectively.

During the temperature ramping stage in the thermal analysis of the oxide precursor mixture prepared from the wet chemical method, endothermic peaks were observed in the differential thermal analysis (DTA) curve (Fig. 1a), while the mass gradually decreased [see the thermogravimetric analysis curve (TGA) in Fig. 1a)] due to the decomposition of $Cu(OH)_2$, $Ni(OH)_2$, $Mg(OH)_2$, $Co(OH)_2$, and $Zn(OH)_2$. However, when the temperature exceeded 450 °C, the mass loss rate significantly decreased. Compared to the XRD pattern of the unheated oxide precursor mixture, peaks corresponding to crystalline oxide phases are evident in the XRD pattern of the mixture heated at 450 °C in addition to signs of amorphous phases (Fig. 1b). It was determined that most of the metal hydroxides had been decomposed. Meanwhile, the metallic elements were distributed evenly in the oxide precursor mixture powder, as shown by the SEM-energy dispersive X-ray spectroscopy (EDS) results in Fig. 1c and d. The powder particle sizes in the oxide precursor mixture treated at 450 °C were distributed narrowly, with most particles measuring less than 1 μm. This could be attributed to the wet chemical process utilized, which allowed for molecular-level mixing of the raw materials, resulting in smaller particles. Therefore, it was inferred that using oxide precursor mixture treated at 450 °C to prepare printing inks would improve the rheological behavior of the inks (due to small particle sizes) and reduce the shrinkage of 3D bodies during sintering processes (owing to the completion of the decomposition of the metal hydroxides).

The rheological behavior of inks was optimized through the addition of additives and adjustment of solid content. All inks exhibited shear thinning behavior and could be considered non-Newtonian fluids, as shown in Fig. 2a. By increasing dispersant content, the viscosity initially increased but then decreased. At 0.4 wt%, ink flowability was excellent due to the steric hindrance and electrostatic stabilization effects of the dispersant [10]. However, excessive dispersant caused flocculation, leading to increased viscosity [10]. The optimal dispersant content was determined to be 0.4 wt% based on experimental results.

The effect of binder content on the thixotropic behavior and viscoelasticity of inks was also studied (Fig. 2b and c). Viscosity increased with binder content due to increased interaction between sodium alginate molecules. Interestingly, increasing binder content also enhanced the shear thinning behavior of the inks, enabling smooth extrusion and rapid thickening [11,12]. At low shear stress, the ink's storage modulus was greater than the loss modulus, indicating dominance of the viscous properties. The flow point of the ink was where the two modulus curves crossed over, with viscous behavior dominating below the flow point and plastic behavior overwhelming above it. The ink with the highest flow point contained 2.2 wt% binder due to increased network stability [13]. Thixotropic behavior was critical for 3D printing, with rebuilding speed determining the ability of the ink to retain its shape after extrusion. The thixotropic index increased with binder content, reaching its maximum at 2.0 wt% binder content, suggesting outstanding rebuilding ability of ink structure. A binder content of 2.0 wt% was selected for ink preparation due to the higher rate of disentanglement of sodium alginate macromolecules by shearing. With an increase in solid content from 77 wt% to 79 wt%, ink viscosity gradually increased due to a reduction in distance between the ceramic powder particles (Fig. 2d). Van der Waals forces also significantly increased.

The inks were printed using a commercial 3D printer (EAZAO). The nozzle size, nozzle speed and extrusion pressure were 1 mm, 10 mm/s and 45 psi, respectively. Fig. 3 displays photos of the printed green bodies with dimensions of 50 × 50 × 10 mm, which indicate the presence of gap flaws in green bodies with a solid content of 79 wt%. Additionally, dimensional accuracy was considerably reduced in these samples. The shear rate distribution model of inks suggests that employing high solid content during printing slows down the inks' passage through the nozzle. Therefore, the viscosity of the inks increased and their extrusion speed was slower than nozzle moving speed, leading to the formation of gaps between the filaments. As the solid content decreases, the extrusion speed of the inks increases, eventually synchronizing with the nozzle speed and enhancing the green body's structure (Fig. 3d–f). Nevertheless, decreasing the solid content further to 77 wt% causes the inks to pile up on either side of the nozzle because of their low viscosity, which leads to an extended rebuilding time after leaving the nozzle. Thus, the optimal solid content was determined to be 78 wt%.

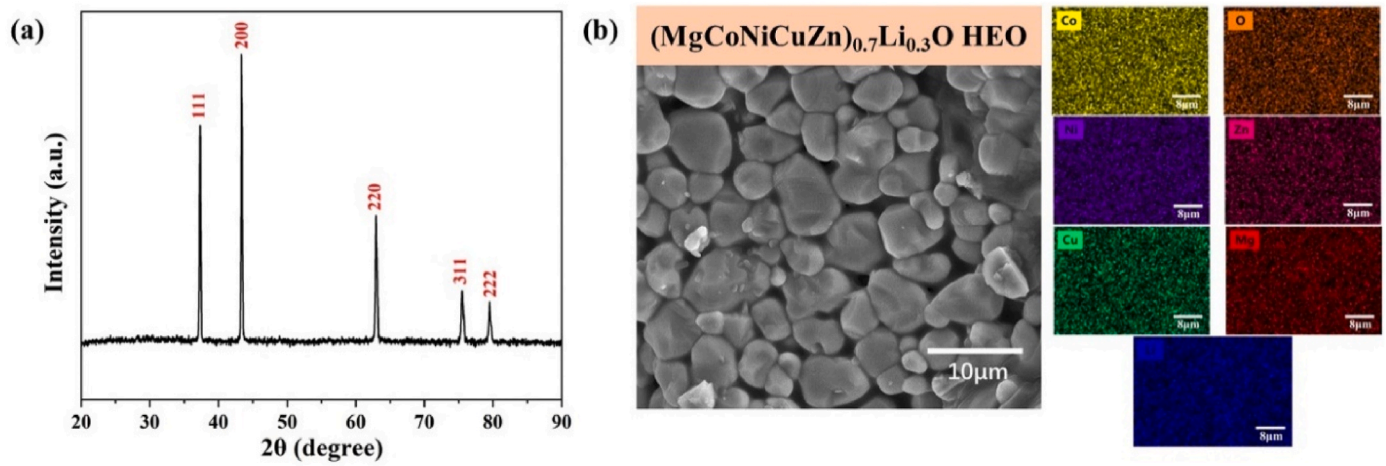

Fig. 4. Phase compositions and morphology of the manufactured $(MgCoNiCuZn)_{0.7}Li_{0.3}O$ HEO treated at 800 °C: (a) XRD patterns; (b) SEM image and EDS mapping.

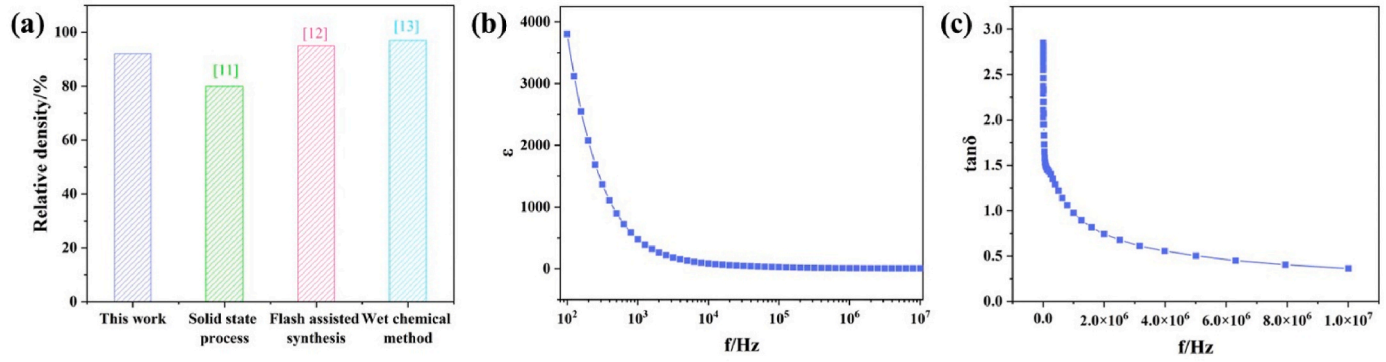

Fig. 5. Properties of manufactured $MgCoNiCuZn)_{0.7}Li_{0.3}O$ HEO: (a) relative density; (b) dielectric constant/ε; (c) loss tangent.

After printed specimens were heated at 800 °C, all diffraction peaks corresponded to the face-centered cubic (FCC) rock-salt crystal system, space group of Fm3m (Fig. 4a). Ellipsoidal-shaped grains were obtained (Fig. 4b) with a grain size of approximately 4 μm for the HEO. The elements of Mg, Co, Ni, Cu, Zn and O were homogeneously distributed in the specimens. The high chemical reactivity of the oxide precursors facilitated the solid solution reaction and led to the production of pure $MgCoNiCuZn)_{0.7}Li_{0.3}O$ HEO with a rock salt structure. Some micron-pores were observed in the matrix, due to ink evaporation and decomposition of binder and dispersant. Properties of the HEO specimens are presented and compared to existing data in Fig. 5. Compared to the previously reported results on (MgCoNiCuZn)O HEO fabricated using traditional techniques [14–16], the relative density of the bulk HEO specimens manufactured in this work remained consistently high. This improvement was attributed to the high solid content of printing inks and the high chemical reactivity of oxide precursors prepared by the wet chemical method. Furthermore, due to the low melting temperature of Li_2CO_3, which is around 714 °C, the heating process would result in the formation of a melting liquid phase. This promoted the formation and growth of the solid solution phase and led to an acceleration of the matrix sintering. However, the specimens exhibited large shrinkage during sintering. The oxide precursors with a high chemical reactivity improved the sintering process, which reduced the porosity and promoted the growth of grains. Equation (2) was used to evaluate the effect of porosity on the dielectric constant (ε) of the specimens.

$$\varepsilon = \varepsilon_m \left[1 - \frac{3P(\varepsilon_m - 1)}{2\varepsilon_m + 1}\right] \quad (2)$$

Where ε_m represents the theoretical dielectric constant, and P is the porosity. It was found that as the porosity increased, the dielectric constant decreased sharply, indicating that the porosity had a great influence on dielectric properties. Owing to the low porosity of the samples and doped Li, manufactured HEO exhibited a high dielectric constant. Furthermore, within the test frequency range of 4.0×10^6 to 1.0×10^7, the loss dielectric of the HEO remained at a low level.

In summary, this study developed and utilized a combination of 3D extrusion-based technique and pressureless sintering to manufacture a high-entropy oxide $MgCoNiCuZn)_{0.7}Li_{0.3}O$. The oxide precursors were obtained through a wet chemical method using metal sulfates. The rheological behavior of the oxide precursor inks was optimized by adjusting the amount of dispersant and binder addition. Finite element simulation was used to establish the relationship between solid content and the ink's printability. The ideal solid composition for printing was determined to be 78 wt% oxide precursors, 0.4 wt% dispersant, and 2.0 wt% binder. Bulk parts were successfully manufactured with high precision at a nozzle size of 1.0 mm, extrusion pressure of 45 psi, and nozzle speed of 10 mm/s. After sintering at 800 °C, the bulk HEO samples exhibited high density and excellent dielectric properties. This 3D extrusion-based technique has a low cost, strong designability, and produces HEOs with high density when compared to traditional manufacturing techniques for HEOs.

Declaration of competing interest

The authors declare that they have no conflict of interest.

Acknowledgements

This work was supported by the Open Foundation of the State Key Laboratory of Refractories and Metallurgy (No.G202204).

Appendix A. Supplementary data

Supplementary data to this article can be found online at https://doi.org/10.1016/j.ceramint.2023.08.061.

References

[1] C. Oses, C. Toher, S. Curtarolo, High-entropy ceramics, Nat. Rev. Mater. 5 (2020) 295–309.
[2] Z. Jin, J. Lyu, Y.L. Zhao, H. Li, Z. Chen, X. Lin, G. Xie, X. Liu, J.J. Kai, H.J. Qiu, Top–down synthesis of noble metal particles on high-entropy oxide supports for electrocatalysis, Chem. Mater. 33 (2021) 1771–1780.
[3] Z. Lin, W. Gao, S. Li, Q. Shen, P. Dai, L. Zou, H. Chen, X. Sun, Effect of in-situ phase transition of (MgCoNiCuZn)O high-entropy oxides on microstructure and performance of Ag-based electrical contact materials, Appl. Surf. Sci. 630 (2023), 157479.
[4] X. Liu, Y. Xing, K. Xu, H. Zhang, M. Gong, Q. Jia, S. Zhang, W. Lei, Kinetically accelerated lithium storage in high-entropy (LiMgCoNiCuZn)O enabled by oxygen vacancies, Small 18 (2022), 2200524.
[5] M. Fu, X. Ma, K. Zhao, X. Li, D. Su, High-entropy materials for energy-related applications, iScience 24 (2021), 102177.
[6] J. Chen, Y. Ling, X. Yu, G. Wang, L. Huang, A. He, Q. Fan, S. Qin, S. Xiang, M. Xu, Z. Han, Water oxidation on CrMnFeCoNi high entropy alloy: improvement through rejuvenation and spin polarization, J. Alloys Compd. 929 (2022), 167344.
[7] Y. Lakhdar, C. Tuck, J. Binner, A. Terry, R. Goodridge, Additive manufacturing of advanced ceramic materials, Progress in Materials Science. Prog. Mater. Sci. 116 (2021), 100736.
[8] T. Yu, X. Zhu, H. Yu, P. Wu, C. Li, X. Han, M. Chen, Material extrusion-based additive manufacturing of zirconia toughened alumina: machinability, mechanical properties and biocompatibility, J. Manuf. Process. 94 (2023) 120–132.
[9] Y. Zhang, Y. Zhang, W. She, L. Yang, G. Liu, Y. Yang, Rheological and harden properties of the high-thixotropy 3D printing concrete, Construct. Build. Mater. 201 (2019) 278–285.
[10] R. Chen, A. Bratten, J. Rittenhouse, T. Huang, W. Jia, M.C. Leu, H. Wen, Additive manufacturing of complexly shaped SiC with high density via extrusion-based technique–Effects of slurry thixotropic behavior and 3D printing parameters, Ceram. Int. 48 (2022) 28444–28454.
[11] S.A. Glukhova, V.S. Molchanov, Y.M. Chesnokov, B.V. Lokshin, E.P. Kharitonova, O.E. Philippova, Green nanocomposite gels based on binary network of sodium alginate and percolating halloysite clay nanotubes for 3D printing, Carbohydr. Polym. 282 (2022), 119106.
[12] C. Voigt, C.G. Aneziris, J. Hubálková, Rheological characterization of slurries for the preparation of alumina foams via replica technique, J. Am. Ceram. Soc. 98 (2015) 1460–1463.
[13] R. Chen, A. Bratten, J. Rittenhouse, M.C. Leu, H. Wen, Additive manufacturing of continuous carbon fiber-reinforced SiC ceramic composite with multiple fiber bundles by an extrusion-based technique, Ceram. Int. 49 (2023) 9839–9847.
[14] C.M. Rost, E. Sachet, T. Borman, C.M. Rost, E. Sachet, T. Borman, A. Moballegh, E. C. Dickey, D. Hou, J.L. Jones, C. Stefano, J.P. Maria, Entropy-stabilized oxides, Nat. Commun. 6 (2015) 8485.
[15] D. Berardan, A.K. Meena, S. Franger, C. Herrero, N. Dragoe, Controlled Jahn-Teller distortion in (MgCoNiCuZn)O-based high entropy oxides, J. Alloys Compd. 704 (2017) 693–700.
[16] M. Biesuz, L. Spiridigliozzi, G. Dell'Agli, M. Bortolotti, V.M. Sglavo, Synthesis and sintering of (Mg, Co, Ni, Cu, Zn)O entropy-stabilized oxides obtained by wet chemical methods, J. Mater. Sci. 53 (2018) 8074–8085.